# Aggregation Kinetics of Colloidal Nanoparticles in a Circulating Microfluidic Cavity

M. R. Barmi[1], B. D. Piorek[1], M. Moskovits[2], C. D. Meinhart[1*]
[1] Department of Mechanical Engineering, University of California Santa Barbara
[2] Department of Chemistry and Biochemistry, University of California Santa Barbara
University of California Santa Barbara, Santa Barbara, CA 03106
* Corresponding author: meinhart@engineering.ucsb.edu

**Abstract:** *COMSOL Multiphysics V4.3* was used to simulate the kinetics of colloidal nanoparticles in a circulating microfluidic cavity. Pressure-driven air flow is directed over the microfluidic cavity, which induces circulating fluid motion in the cavity. Analyte contained in the air stream is absorbed into the cavity, mixes as a result of the circulating cavity flow, and interacts with the nanoparticles. As a result, the nanoparticles sequentially aggregate into clusters of higher orders. This process is highly non-linear. Our numerical model captures the following physical phenomena: (1) fluid dynamics of the air flow, (2) fluid dynamics of the microfluidic cavity, and (3) second order aggregation kinetics. In addition, at the interface, we account for momentum transport, heat transfer, mass transport through evaporation-driven phase change, and mass transport through analyte adsorption.

To control the evaporation rate from the interface, the temperature of the cavity and relative humidity of the air are specified. The energy equation and diffusion-convection of water vapor into air are added to the model to calculate the evaporation rate. We consider the effect of nanoparticle concentration in the cavity to find the optimum condition to get the highest number of the dimers in the cavity. The final result for concentration of the aggregates in ambient condition $T_\infty$ = 20°C and $RH$ = 50%, wall temperature $T_w$ = 10°C, inlet velocity $u_{in}$ = 10 mm/s, analyte concentration $c_a$ = 1 mM, the dimer concentration reaches a maximum at around $t \sim 100$s. At larger times, the number of dimers decreases as higher order aggregates form, and the available monomers decreases. In the case of efficient mixing inside of the cavity, there is an optimum point at $\hat{t}_{opt} = kc_{NP}t \approx 0.7$ where the number of formed dimers is maxima.

**Keywords:** Chemical Detection, SERS, Aggregation Kinetics, Evaporation.

**Nomenclature**

| Name | Unit | Description |
|---|---|---|
| $V_0$ | J | Aggregation barrier |
| $\beta$ | $K^{-1}$ | Aggregation coefficient |
| $k$ | $M^{-1}s^{-1}$ | Aggregation rate |
| $k_B$ | $J.K^{-1}$ | Boltzmann constant |
| $c$ | M | Concentration |
| $F$ | - | Curvature |
| $\rho$ | $Kg.m^{-3}$ | Density |
| $D$ | $m^2.s^{-1}$ | Diffusion coefficient |
| $\mu$ | $m^2.s^{-1}$ | Dynamic viscosity |
| $R$ | $J.kg^{-1}mol^{-1}$ | Gas constant |
| $k_H$ | - | Henry's constant |
| $k_0$ | $M^{-1}.s^{-1}$ | Maximum aggregation rate |
| $p$ | Pa | Pressure |
| $R_c$ | m | Radius of curvature |
| $R_i$ | $M.s^{-1}$ | Reaction rate |
| $\gamma$ | $N.m^{-1}$ | Surface tension |
| $T$ | K | Temperature |
| $k$ | $W.m^{-1}.K^{-1}$ | Thermal conductivity |
| $p_v$ | Pa | Vapor pressure |
| $u$ | $m.s^{-1}$ | Velocity field |

**Subscripts and Superscripts**

| | |
|---|---|
| $\infty$ | Ambient |
| $g$ | Gas |
| $i$ | interface |
| $w$ | Liquid |
| $n$ | Normal to surface |
| $a$ | Analyte |
| $1$ | Monomer |
| $2$ | Dimer |
| $3$ | Trimer |
| $4$ | Tetramer |

## 1. Introduction

Raman spectroscopy uses inelastic interactions between a monochromatic light and molecules to detect and identify the molecular structure like a 'finger print' [1]. Surface Enhanced Raman Spectroscopy (SERS), which takes advantage of surface plasmons on rough metal surfaces, such as silver or gold nanoparticles, can be used to

amplify the Raman signal [2-5]. At points of high surface curvature, the electric field is particularly high, creating so-called 'SERS hotspots'. The signal in the hotspot is enhanced significantly, thereby enabling the detection of even single molecules [6-8]. In the past 40 years, Raman spectroscopy and SERS have been utilized as powerful tools for detection and identification of different chemical and biological agents [9-13]. However, aggregation does not happen readily for some molecules. To stimulate aggregation, we use a cavity inside of a microchannel filled with the silver sol, which can absorb airborne analyte to induce aggregation. The air velocity makes a circulating flow inside of the cavity which helps to mix analyte and silver sol to increase the aggregation rate. The aggregation process is highly non-linear and described by a system of equations. Our numerical model accounts for the fluid dynamics of the air flow, fluid dynamics in the cavity, and second order aggregation kinetics. In addition, at the interface, we account for momentum transport, heat transfer, mass transport through evaporation-driven phase change, and mass transport through analyte adsorption. This highly non-linear system of equations is solved using *COMSOL v4.3* to find the concentration of formed dimers based on the initial concentration of silver nanoparticles inside of the cavity.

## 2. Use of COMSOL Multiphysics

Due to the complexity of this problem, we consider the 2D model for the cavity. The computational domain is shown in Figure 1. Air contains analyte at concentration $c_0$ flows through the microchannel at a fully-developed $u_0$ velocity at ambient condition $T_\infty$ and relative humidity *RH%*. The silver sol inside of the cavity absorbs analyte which induces the aggregation of silver nanoparticles based on rate equations, $R_i$. The air velocity makes a circulating flow inside the cavity which helps to mix analyte and silver sol to increase the aggregation rate. The concentration of formed dimers depends on the aggregation rate, which is determined by the analyte concentration. We investigate flow field, mass transport, and aggregation kinetics to determine the number of formed dimers.

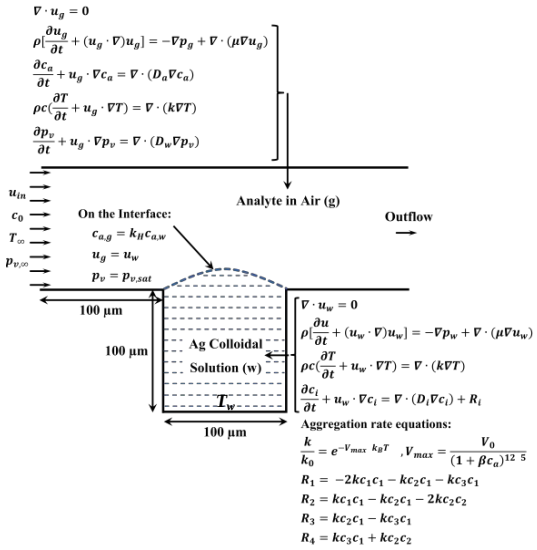


**Figure 1**. Computational Domain and governing equations. Air flow containing airborne analyte flows over the Ag colloidal solution in the cavity. The silver sol absorbs analyte according to Henry's law. The absorbed analyte stimulates the aggregation process between silver nanoparticles causes formation of 'hot spots' for chemical detection. The position of the interface is controlled by evaporation rate based on temperature, relative humidity and air velocity.

The initial curvature of the aqueous solution depends on the surface tension and is determined by 1-D Poisson's equation as,

$$2R_c = \frac{F_{xx}}{(1 + F_x^2)^{1/2}}$$

where the radius of curvature is $R_c = dp/2\gamma$. By solving this equation over the interface along with deformed geometry, we can find the shape of the interface. For boundary conditions on the edges of the interface, we apply $F = 0$ which implies pinned points of the interface.

The fluid flows in each domain are governed by the continuity and Navier-Stokes equations as,

$$\nabla \cdot \mathbf{u} = 0$$

$$\rho\left[\frac{\partial u}{\partial t} + (\mathbf{u} \cdot \nabla)u\right] = -\nabla p + \nabla \cdot (\mu \nabla u)$$

We apply no-slip boundary condition on all walls. On the interface, we apply slip condition for gas phase and the resulting velocity is equal to the velocity for the liquid phase. The mass

transport of the analyte is modeled using a convection-diffusion equation in air,

$$\frac{\partial c_a}{\partial t} + \mathbf{u} \cdot \nabla c_a = \nabla \cdot (D_a \nabla c_a)$$

along with a weak formulation over the boundary to calculate absorbed analyte by water according to Henry's law as,

$$c_{a,g} = k_H c_{a,w}$$

In our simulation, we assume that $D_a = 10^{-6}$ [$m^2/s$] and $k_H = 0.5$.

Water can evaporate from the interface due to diffusion of water vapor into air, which depends on the temperature and relative humidity. Therefore, we include the energy equation and convection-diffusion equation of water vapor to calculate evaporation rate from the interface.

$$\frac{\partial T}{\partial t} + \mathbf{u} \cdot \nabla T = \nabla \cdot (k \nabla T)$$

$$\frac{\partial p_v}{\partial t} + \mathbf{u} \cdot \nabla p_v = \nabla \cdot (D_w \nabla p_v)$$

To calculate evaporation rate, the deformed geometry module is added to the numerical model to find moving water/air interface during the evaporation. The interface shape is controlled by surface tension and gravity through Bond number, $Bo=(gL^2(\rho_w-\rho_g))/\sigma$, which accounts for the balance of surface tension and gravitational force on the droplet shape. Here the Bond number is in the range of 0.05 ~ 0.1. Therefore the interface is assumed spherical during evaporation which means that the interface follows $y = (R_c^2-x^2)^{1/2} \pm (R_c-h)$ where "+" is for $h < 0$ and "–" is for $h > 0$. The interface recedes inward according to the evaporation rate in each time step. The velocity of the interface, $u_i$ is illustrated in Figure 2.

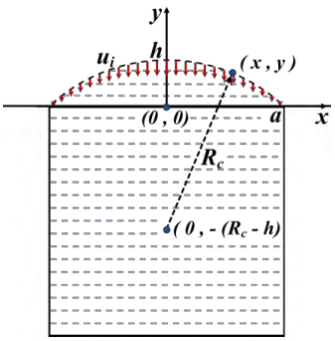


**Figure 2**. Cavity and the moving interface with vertical velocity $u_i$ based on evaporation rate

The average evaporation rate can be calculated by integration of evaporation flux along the water/air interface, *S(t)*,

$$\frac{dV}{dt} = -\frac{J_e}{\rho} = -\int_{S(t)} \frac{M_w D}{\rho RT} \nabla_n p_v dl$$

The interface velocity is vertical due to the pinned contact-line at the corner of the cavity and can be calculated by,

$$u_i = -\frac{dy}{dt} = -\frac{dy}{dR_c}\frac{dR_c}{dt} - \frac{dy}{dh}\frac{dh}{dt}$$

The area, $A = \frac{4}{3}ah + \frac{h^3}{4a}$, and radius of curvature, $R_c = \frac{h}{2} + \frac{a^2}{2h}$ of the cap depend on the droplet height, $h$, and the constant contact-line radius, $a$. Therefore,

$$\frac{dh}{dt} = \frac{12a}{16a^2 + 9h^2}\frac{dA}{dt}$$

$$\frac{dR_c}{dt} = \frac{1}{2}\left(1 - \frac{a^2}{h^2}\right)\frac{dh}{dt}$$

And finally, from the analytical expression for the interface,

$$\frac{dz}{dR_c} = R_c\left({R_c}^2 - r^2\right)^{-1/2} \pm 1$$

$$\frac{dz}{dh} = \pm 1$$

where "+" is for $h < 0$ and "–" is for $h > 0$.

Therefore, we can calculate velocity field, temperature distribution as well as evaporation rate from the interface. Now, we can consider the

effect of different parameters on the aggregation kinetics inside of the cavity. The aggregation kinetics equation is given by Moskovits and Vlčková [7] as,

$$\frac{k}{k_0} = e^{-V_{max}/k_BT} \quad , V_{max} = \frac{V_0}{(1+\beta c_a)^{12/5}}$$

where the maximum aggregation rate $k_0$ and the potential barrier $V_0$ are constant, the factor $\beta$ depends on temperature, and $c_a$ is the concentration of the analyte in solution. For a typical analyte we assume $k_0 = 10^8$ [$M^{-1}s^{-1}$], $V_0 = 3k_BT$ and $\beta = 10^4$ [$M^{-1}$].

The convection-diffusion equation is taken into account to find the concentration of analyte and formed aggregates:

$$\frac{\partial c_i}{\partial t} + \mathbf{u} \cdot \nabla c_i = \nabla \cdot (D_i \nabla c_i) + R_i$$

where the reaction rate can be calculated from,

$$R_a = 0$$

$$R_1 = -2kc_1c_1 - kc_2c_1 - kc_3c_1$$

$$R_2 = kc_1c_1 - kc_2c_1 - 2kc_2c_2$$

$$R_3 = kc_2c_1 - kc_3c_1$$

$$R_4 = kc_3c_1 + kc_2c_2$$

where $i$ indicates the species as follows: $i = a$ for analyte, $i = 1$ for colloid monomers, $i = 2$ for dimers, and so on for first four orders of aggregates. The diffusion coefficient, $D_i$, of each species in laminar flow is taken as $D_a = 10^{-10}$ [$m^2/s$] for the analyte, and $D_i = 10^{-11}$ [$m^2/s$] for colloid monomers and aggregates. The initial conditions for the analyte is $c_a = c_0$ at the inlet and $c_a = 0$ in the cavity. Also, we specify the initial conditions for the aggregates as $c_1 = c_{NP}$ and $c_2 = c_3 = c_4 = 0$ in the cavity.

Finally, we can define non-dimensional time and concentration to compare the results as,

$$\hat{c}_i = \frac{c_i}{c_{NP}} \quad , \quad \hat{t} = k\, c_{NP} t$$

To solve these equations, the physics shown in Table 1 are added to COMSOL multiphysics.

**Table 1**- Multiphysics model

| *Physics* | *D* | *Variables* | *Domain* |
|---|---|---|---|
| **Weak form PDE** | 1D | $F$ | Interface |
| **Deformed Geometry** | 2D | $X, Y$ | Entire |
| **Laminar Flow 1** | 2D | $u_g, v_g, p_g$ | Air |
| **Laminar Flow 2** | 2D | $u_w, v_w, p_w$ | Liquid |
| **Heat Transfer** | 2D | $T$ | Entire |
| **Transport of Diluted Species** | 2D | $p_v$ | Air |
| **Weak form PDE** | 1D | $c_{BC}$ | Interface |
| **Transport of Diluted Species** | 2D | $c_a$ | Air |
| **Transport of Diluted Species** | 2D | $c_a, c_1, c_2, c_3, c_4$ | Liquid |

## 3. Results and Discussions

To consider mesh dependency, the problem is solved for different mesh sizes. The criteria for mesh is the conservation of number of nanoparticles in formed aggregates as,

$$c_1 + 2c_2 + 3c_3 + 4c_4 = c_{NP}$$

At low mesh sizes, there are mass fluxes from the interface that does not satisfy the conservation of nanoparticles. The following mesh is chosen, which consists of $10^5$ elements. The mesh size is refined close to the walls and interface to capture sharp gradients.

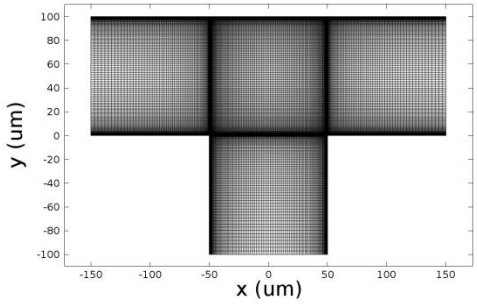


**Figure 3**. Mesh consisted of $10^5$ elements

The solution of Poisson's equation along with the moving geometry determines the initial curvature of the interface which becomes the initial geometry for the rest of the modeling.

The flowing air carries airborne analyte through the microchannel. In addition, it causes circulation inside of the cavity which helps the mixing of the nanoparticles and absorbed analyte

from the interface inducing aggregation. The concentration of formed dimers in the cavity in different times is demonstrated in Figure 4.

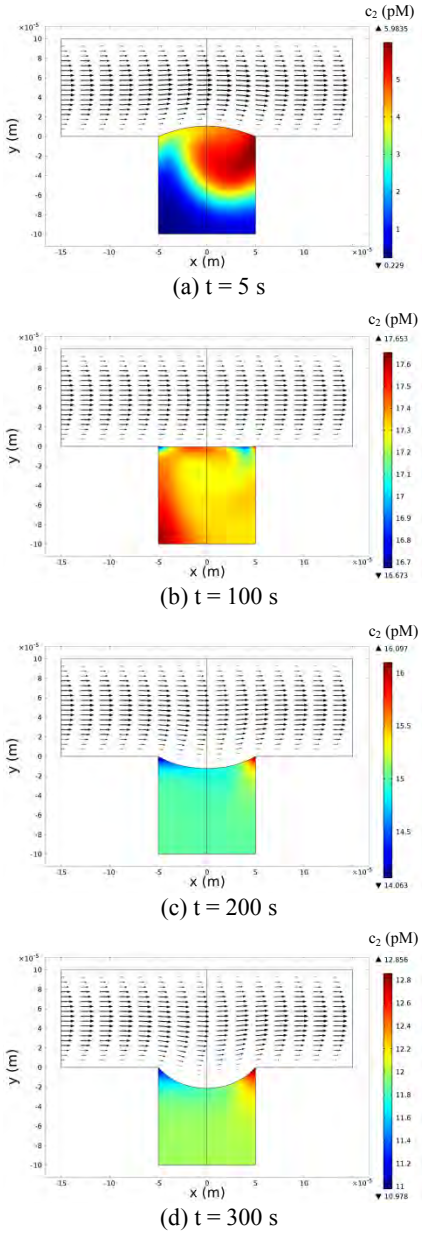


**Figure 4.** Formation of dimers in the cavity and movement of the interface due to evaporation for $T_\infty$ = 20°C, $T_w$ = 10°C, $RH$ = 50%, inlet velocity $u_{in}$ = 10 mm/s, analyte concentration $c_a$ = 1 mM, and initial concentration of nanoparticle $c_{NP}$ = 100 pM.

The simulation is performed for the following parameters:

- Ambient condition:
  - Ambient temperature: $T_\infty$ = 20°C
  - Cavity wall temperature: $T_w$ = 10°C
  - Relative humidity: $RH$ = 50%
- Inlet velocity: $u_{in}$ = 10 mm/s
- Analyte concentration: $c_a$ = 1 mM
- Nanoparticle concentration: $c_{NP}$ = 100 pM

The non-dimensional concentrations of formed aggregates as a function of non-dimensional time are shown in Figure 5. The concentration of formed dimers depends on the initial concentration of nanoparticles. However, due to the efficient mixing inside of the cavity, the non-dimensional concentration of dimers ($c_2/c_{NP}$) is independent of the initial concentration of nanoparticles. According to Figure 5, the maximum concentration of dimers happen at $\hat{t} = k\, c_{NP} t \approx 0.7$, which can be used to determine the best conditions for optimum chemical detection.

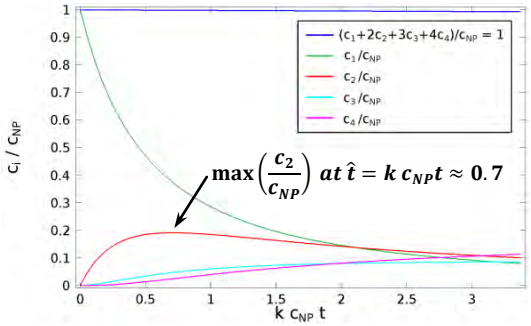


**Figure 5-** Formation of aggregates and the condition for maximum concentration of formed dimers

## 4. Conclusion

*COMSOL Multiphysics V4.3* is used to simulate the kinetics of colloidal nanoparticles in a circulating microfluidic cavity. Analyte contained in the air stream is absorbed into the cavity, mixes as a result of the circulating cavity flow, and interacts with the nanoparticles. As a result, the nanoparticles sequentially aggregate into clusters of higher orders.

We investigate the flow field, mass transport and aggregation kinetics to find the number of formed dimers according to the concentration of the analyte. There is an optimum point at $\hat{t}_{opt} = kc_{NP}t \approx 0.7$ where the number of formed dimers is maxima.

## 5. Acknowledgements

This work was supported by the Institute for Collaborative Biotechnologies through grant W911NF-09-0001 from the U.S. Army Research Office. The content of the information does not necessarily reflect the position or the policy of the Government, and no official endorsement should be inferred.

## 6. References

1 Moskovits, M., Surface roughness and the enhanced intensity of Raman scattering by molecules adsorbed on metals, *The Journal of Chemical Physics,* **69**, 4159 (1978).

2 Kerker, M., Wang, D., Chew, H., Surface enhanced Raman scattering (SERS) by molecules adsorbed at spherical particles, *Applied Optics,* **19**, 4159–4174 (1980).

3 Kerker, M., Electromagnetic model for surface-enhanced Raman scattering (SERS) on metal colloids, *Accounts of Chemical Research*, **17**, 271–277 (1984).

4 Kneipp, K., Wang, Y., Kneipp, H., Perelman, L., Itzkan, I., Dasari, R., Feld, M. Single molecule detection using surface-enhanced Raman scattering (SERS) *Physical Review Letters,* **78**, 1667–1670 (1997).

5 Qian, X., Nie, S., Single-molecule and single-nanoparticle SERS: from fundamental mechanisms to biomedical applications, *Chemical Society Reviews,* **37**, 912–920 (2008).

6 Moskovits, M., Tay, L., Yang, J., Haslett, T., Surface enhanced Raman: a report from near-field, *Optical properties of nanostructured random media,* 215–227 (2002).

7 Moskovits, M.; Vlcková, B., Adsorbate-induced silver nanoparticle aggregation kinetics, *The Journal of Physical Chemistry B*, **109**, 14755–14758 (2005).

8 Maher, R., Galloway, C., Le Ru, E., Cohen, L., Etchegoin, P., Vibrational pumping in surface enhanced Raman scattering (SERS), *Chem. Soc. Rev.,* **37**, 965–979 (2008).

9 Piorek, B., Lee, S., Santiago, J., Moskovits, M., Banerjee, S., Meinhart, M., Free-surface microfluidic control of surface-enhanced Raman spectroscopy for the optimized detection of airborne molecules, *Proceedings of the National Academy of Sciences,* **104**, 18898 (2007).

10 Cotton, T., Kim, J., Chumanov, G., Application of surface-enhanced Raman spectroscopy to biological systems, *Journal of Raman spectroscopy,* **22**, 729–742 (1991).

11 Nabiev, I., Chourpa, I., Manfait, M., Applications of Raman and surface-enhanced Raman scattering spectroscopy in medicine, *Journal of Raman Spectroscopy*, **25**, 13–23 (1994).

12 Hering, K., Cialla, D., Ackermann, K., Dörfer, T., Möller, R., Schneidewind, H., Mattheis, R., Fritzsche, W., Rösch, P., Popp, J., SERS: a versatile tool in chemical and biochemical diagnostics, *Analytical and bioanalytical chemistry*, **390**, 113–124 (2008).

13 Chiu, T., Huang, C., Aptamer-Functionalized Nano-Biosensors, *Sensors*, ***9***, 10356–10388 (2009).

14 Hu, H., Larson, R., Analysis of the effects of Marangoni stresses on the microflow in an evaporating sessile droplet, *Langmuir*, **21**, 3972–3980 (2005).

15 Hu, H., Larson, R., Evaporation of a sessile droplet on a substrate, *The Journal of Physical Chemistry B,* **106**, 1334–1344 (2002).

16 Girard, F., Antoni, M., Sefiane, K., On the effect of Marangoni flow on evaporation rates of heated water drops, *Langmuir*, **24**, 9207–9210 (2008).